

Rotating wormholes in Einstein-Dirac-Maxwell theory

Vladimir Dzhunushaliev^{1,2,3,*} and Vladimir Folomeev^{2,3,†}

¹*Department of Theoretical and Nuclear Physics,
Al-Farabi Kazakh National University, Almaty 050040, Kazakhstan*

²*Institute for Experimental and Theoretical Physics,
Al-Farabi Kazakh National University, Almaty 050040, Kazakhstan*

³*Academician J. Jeenbaev Institute of Physics of the NAS of the
Kyrgyz Republic, 265 a, Chui Street, Bishkek 720071, Kyrgyzstan*

(Dated: April 21, 2026)

We consider rotating wormhole solutions in general relativity supported by a complex non-phantom spinor field (which provides a nontrivial spacetime topology) and electromagnetic fields. The solutions are asymmetric, regular, asymptotically flat and carry nonzero total angular momentum. The physical properties of the resulting configurations are completely determined by the values of three input quantities: the throat parameter, the spinor frequency, and the electromagnetic coupling constant. The wormholes connect two identical Minkowski spacetimes possessing in general different masses and global charges.

Keywords: rotating wormholes, spinor, electric, and magnetic fields

I. INTRODUCTION

Wormholes are hypothetical strongly gravitating objects possessing a nontrivial spacetime topology. It is assumed that they can connect either two distant points in one universe or even different universes [1, 2]. The literature in the field offers a variety of objects of this type. Most frequently one considers the simplest static (spherically symmetric) configurations within general relativity (see, e.g., the pioneering works [3–7]). In this case a necessary ingredient providing a wormhole topology is some exotic (or phantom) matter certainly violating the weak and null energy conditions, at least near the throat [1, 7, 8]. Such static systems can be generalized to the case with the presence of rotation (axially symmetric configurations) [9–15], but the use of phantom matter is nevertheless necessary. On the other hand, it is possible to avoid this necessity (phantom-free wormholes), but this is achieved, for instance, either at the cost of modifying gravity [16–19], or of considering systems with cylindrical symmetry within general relativity [20, 21] (at the cost of the absence of asymptotic flatness; see, however, Refs. [22, 23] where regular asymptotically flat cylindrical wormholes are obtained by introducing two junction surfaces, between which a wormhole throat is located and to which two flat external regions are matched), or of considering axially symmetric vacuum solutions, such as the Kerr metric with large angular momenta [1] and Zipoy’s static solution [24] (which contain a ring singularity).

It is therefore of interest to try to find spherically or axially symmetric asymptotically flat wormhole-like solutions while remaining within general relativity but without dealing with any exotic matter. In particular, Ref. [25] considers static, *symmetric* with respect to the wormhole throat solutions within Einstein-Dirac-Maxwell theory. However, those solutions have certain features (for instance, the introduction of a thin shell is needed) that were criticized in the papers [26–28]. As a possibility to avoid the weaknesses of the model of Ref. [25], the pioneering work [28], also within Einstein-Dirac-Maxwell theory, suggests static *asymmetric* wormholes supported by smooth metric and matter (classical spinor and electric) fields without invoking any thin shells, and the spinor field is a non-phantom field.

In the present paper we generalize the results of Ref. [28] to the case of rotating wormholes supported by spinor and electromagnetic fields (see also Ref. [29] where a new family of nonrotating solutions within Einstein-Dirac-Maxwell theory has been obtained). In doing so, we impose rotation on the complex non-phantom spinor field in the same way that rotation is imposed for a complex spinor field in constructing spinning Dirac stars [30, 31]. Thus the *Ansatz* for the complex spinor field has an explicit dependence on the azimuthal number featuring a half-integer parameter M_ψ . The rotating wormhole solutions then do not only possess a mass and a Noether charge but they also carry an angular momentum proportional to the Noether charge with a proportionality coefficient M_ψ , a relation known from the spinning Dirac stars [30, 31]. To the best of our knowledge, the configurations considered in the present paper are the first example of rotating asymptotically flat wormholes with a non-phantom spinor field.

* v.dzhunushaliev@gmail.com

† vfolomeev@mail.ru

Notice here that in the present paper we consider a system involving a classical spinor field. However, a consideration of self-gravitating fermions still remains somewhat obscure, since a spinor field must be treated in terms of a normalizable quantum wave function. Nevertheless, one can impose certain restrictions by considering only one-particle fermion states and by ignoring second quantization of the fields. In this framework gravitational interaction can be treated purely classically. In this case the set of the Einstein-Dirac equations describes regular localized solitonic configurations [32], the so-called Dirac stars [30, 31, 33–35], as well as wormhole systems mentioned above [25, 28]. Consistent with this, here we follow Ref. [36] where the conclusion has been drawn that a classical spinor field may appear either as a result of some effective description of a more complex quantum system or when a quantum state of a spinor is in some sense “close” to a vacuum state where a classical consideration of a massive Dirac spinor may be a good approximation. In doing so, it is assumed that the spinor field represents a set of four complex-valued spacetime functions which transform according to the spinor representation of the Lorentz group [36].

The paper is organized as follows. In Sec. II, we present the action, *Ansätze*, and field equations for the configurations under consideration. In Sec. III A, we write down asymptotic expressions for the field functions and the corresponding boundary conditions, using which we solve the equations numerically in Sec. III D for neutral and charged spinor fields. Finally, in Sec. IV, we summarize and discuss the results obtained.

II. THE MODEL

The total action for the system can be written in the form [we use the metric signature $(+, -, -, -)$ and natural units $c = \hbar = 1$]

$$S_{\text{tot}} = -\frac{1}{16\pi G} \int d^4x \sqrt{-g} R + S_{\text{sp}} + S_{\text{EM}}, \quad (1)$$

where G is the Newtonian gravitational constant, R is the scalar curvature, and g is the determinant of the metric; S_{sp} and S_{EM} denote the actions of spinor, ψ , and electromagnetic, A_μ , fields, respectively. The action for the electromagnetic field can be found from the Lagrangian

$$L_{\text{EM}} = -\frac{1}{4} F_{\mu\nu} F^{\mu\nu},$$

where the electromagnetic field tensor is $F_{\mu\nu} = \partial_\mu A_\nu - \partial_\nu A_\mu$ with $\mu, \nu = 0, 1, 2, 3$ being spacetime indices.

In turn, the action S_{sp} for the spinor field ψ appearing in Eq. (1) can be obtained from the Lagrangian

$$L_{\text{sp}} = \frac{i}{2} (\bar{\psi} \gamma^\mu \psi_{;\mu} - \bar{\psi}_{;\mu} \gamma^\mu \psi) - m_s \bar{\psi} \psi,$$

where m_s is the mass of the spinor field and the semicolon denotes the covariant derivative defined as $\psi_{;\mu} = [\partial_\mu + 1/8 \omega_{ab\mu} (\gamma^a \gamma^b - \gamma^b \gamma^a) + ie A_\mu] \psi$ with a, b being tetrad indices. Here γ^a are the Dirac matrices in the Weyl representation in flat space,

$$\gamma^0 = \begin{pmatrix} 0 & 1 \\ 1 & 0 \end{pmatrix}, \quad \gamma^k = \begin{pmatrix} 0 & \sigma^k \\ -\sigma^k & 0 \end{pmatrix},$$

where $k = 1, 2, 3$ and σ^k are the Pauli matrices. In turn, the Dirac matrices in curved space, $\gamma^\mu = e_a^\mu \gamma^a$, are derived using the tetrad e_a^μ , and $\omega_{ab\mu}$ is the spin connection [for its definition, see Ref. [37], Eq. (7.135)]. The gauge coupling constant e describes the minimal interaction between the electromagnetic and spinor fields.

Then, by varying the action (1) with respect to the metric, the spinor field, and the vector potential A_μ , we derive the Einstein, Dirac, and Maxwell field equations in curved spacetime:

$$E_\mu^\nu \equiv R_\mu^\nu - \frac{1}{2} \delta_\mu^\nu R - 8\pi G T_\mu^\nu = 0, \quad (2)$$

$$i \gamma^\mu \psi_{;\mu} - m_s \psi = 0, \quad (3)$$

$$i \bar{\psi}_{;\mu} \gamma^\mu + m_s \bar{\psi} = 0, \quad (4)$$

$$\frac{1}{\sqrt{-g}} \frac{\partial}{\partial x^\nu} (\sqrt{-g} F^{\mu\nu}) = -e j^\mu, \quad (5)$$

where $j^\mu = \bar{\psi} \gamma^\mu \psi$ is the four-current of the spinor field. The equation (2) involves the energy-momentum tensor T_μ^ν , which can be written in a symmetric form as

$$T_\mu^\nu = \frac{i}{4} g^{\nu\rho} [\bar{\psi} \gamma_\mu \psi_{;\rho} + \bar{\psi}_{;\rho} \gamma_\mu \psi - \bar{\psi}_{;\mu} \gamma_\rho \psi - \bar{\psi}_{;\rho} \gamma_\mu \psi] - F^{\nu\rho} F_{\mu\rho} + \frac{1}{4} \delta_\mu^\nu F_{\alpha\beta} F^{\alpha\beta}. \quad (6)$$

Since we consider here axially symmetric configurations, we use the following line element for a stationary, axially symmetric spacetime [11, 12, 14]:

$$ds^2 = e^f dt^2 - e^{q-f} \left[e^b (dr^2 + hd\theta^2) + h \sin^2 \theta (d\varphi - \omega dt)^2 \right], \quad (7)$$

where the metric functions f, q, b , and ω depend solely on the radial coordinate r and the polar angle θ , and the auxiliary function $h = r^2 + r_0^2$ contains the throat parameter r_0 ; the radial coordinate r covers the range $-\infty < r < +\infty$. The z -axis ($\theta = 0$) represents the symmetry axis of the system. Asymptotically (as $r \rightarrow \pm\infty$), the functions $f, q, b, \omega \rightarrow 0$; i.e., the spacetime approaches Minkowski spacetime. In what follows, we employ the following orthonormal tetrad for the metric (7):

$$\mathbf{e}_\mu^0 dx^\mu = e^{f/2} dt, \quad \mathbf{e}_\mu^1 dx^\mu = e^{(b-f+q)/2} dr, \quad \mathbf{e}_\mu^2 dx^\mu = e^{(b-f+q)/2} \sqrt{h} d\theta, \quad \mathbf{e}_\mu^3 dx^\mu = e^{(q-f)/2} \sqrt{h} \sin \theta (d\varphi - \omega dt),$$

such that $ds^2 = \eta_{ab} (\mathbf{e}_\mu^a dx^\mu) (\mathbf{e}_\nu^b dx^\nu)$ with $\eta_{ab} = \text{diag}(1, -1, -1, -1)$.

The spinor field is parameterized by two complex functions [30, 31, 38]

$$\psi^T = e^{i(M_\psi \varphi - \Omega t)} (\psi_1, \psi_2, \psi_2^*, \psi_1^*). \quad (8)$$

Here the spinor frequency Ω is the eigenvalue of the Dirac Hamiltonian, M_ψ is a half-integer parameter (the azimuthal number; in what follows, we take $M_\psi = 1/2$). For our purposes, it is convenient to represent the components of the spinor field (8) as

$$\psi_1 = \frac{1}{2} [X + Y + i(V + W)], \quad \psi_2 = \frac{1}{2} [X - Y + i(V - W)],$$

where the four real functions X, Y, V , and W depend only on the coordinates r and θ .

The gauge field is parameterized by an electric, ϕ , and a magnetic, σ , potentials

$$A_\mu = \{\phi(r, \theta), 0, 0, \sigma(r, \theta)\}. \quad (9)$$

Hence, the electric field \mathbf{E} and the magnetic field \mathbf{H} as measured by the zero-angular-momentum observer (ZAMO) are given by

$$\begin{aligned} E_\beta &= F_{\alpha\beta} n^\alpha = \left(0, -e^{-f/2} \left[\frac{\partial\phi}{\partial r} + \omega \frac{\partial\sigma}{\partial r} \right], -e^{-f/2} \left[\frac{\partial\phi}{\partial\theta} + \omega \frac{\partial\sigma}{\partial\theta} \right], 0 \right), \\ H_\beta &= -\frac{1}{2} \epsilon_{\alpha\beta\mu\nu} n^\alpha F^{\mu\nu} = \left(0, \frac{1}{h} e^{(f-q)/2} \csc\theta \frac{\partial\sigma}{\partial\theta}, -e^{(f-q)/2} \csc\theta \frac{\partial\sigma}{\partial r}, 0 \right), \end{aligned} \quad (10)$$

where n^α is the four-velocity vector of the ZAMO, which in our case is

$$n^\alpha = \sqrt{g^{tt}} \left(1, 0, 0, \frac{g^{t\varphi}}{g^{tt}} \right) = e^{-f/2} (1, 0, 0, \omega).$$

Then, substituting the *Ansätze* (8) and (9) and the metric (7) in the field equations (2), (3), and (5), one can obtain the set of field equations given in Appendix A. In addition to the Einstein equations (A2)-(A5), which are elliptic partial differential equations, one has two more equations of gravitation $E_\theta^x = 0$ and $d \equiv (E_x^x - E_\theta^\theta) = 0$, whose structure is not of Laplace form (here the index x denotes a dimensionless radial coordinate introduced in Appendix A); they may be regarded as ‘‘constraints.’’ The numerical calculations given below show that the first constraint equation is always satisfied automatically, whereas the adjustment of the corresponding asymptotic value of the electric field is required to satisfy the second constraint (see below in Sec. III C).

III. NUMERICAL SOLUTIONS

In this section, we numerically solve the equations (A2)-(A11) and discuss the physical properties of the configurations under consideration.

A. Asymptotic behaviour and boundary conditions

The far field asymptotic of the Maxwell equations (A6) and (A7) is of the form

$$\bar{\phi} \approx \bar{\phi}_{\pm\infty} + \frac{\bar{Q}_{\pm}}{x} + \dots, \quad \bar{\sigma} \approx -\frac{\bar{\mu}_{m\pm}}{x} \sin^2 \theta + \dots, \quad (11)$$

where $\bar{\phi}_{\pm\infty}$ are two integration constants corresponding to the values of the electric field potential as $x \rightarrow \pm\infty$, respectively, and $\bar{Q}_{\pm} \equiv \sqrt{G/4\pi} m_s Q_{\pm}$ represents the charge of the systems located to the left (\bar{Q}_{-}) and to the right (\bar{Q}_{+}) of the center. Since the integration constants $\bar{\phi}_{\pm\infty}$ are arbitrary, for calculations given below, we take the constant $\bar{\phi}_{-\infty} = 0$, whereas the constant $\bar{\phi}_{+\infty}$ is so adjusted that the constraint equation $d \equiv (E_x^x - E_{\theta}^{\theta}) = 0$ is satisfied. In turn, $\bar{\mu}_{m\pm} \equiv \sqrt{G/4\pi} m_s^2 \mu_{m\pm}$ is a corresponding dimensionless magnetic moment. Consequently, these quantities can be read off from the asymptotic subleading behaviour of (11) as

$$\bar{Q}_{\pm} = - \lim_{x \rightarrow \pm\infty} x^2 \frac{\partial \bar{\phi}}{\partial x} = -\frac{c_k}{4} \lim_{\bar{x} \rightarrow \pm 1} \frac{\partial_{\bar{x}} \bar{\phi}}{1 - \bar{x}^2}, \quad \bar{\mu}_{m\pm} = \lim_{x \rightarrow \pm\infty} \frac{x^2}{\sin^2 \theta} \frac{\partial \bar{\sigma}}{\partial x} = \frac{c_k}{4} \lim_{\bar{x} \rightarrow \pm 1} \frac{1}{\sin^2 \theta} \frac{\partial_{\bar{x}} \bar{\sigma}}{1 - \bar{x}^2}, \quad (12)$$

where the last expressions in the above equations represent the quantities under consideration in terms of the compactified coordinate \bar{x} from Eq. (20).

In turn, asymptotic flatness of the spacetime implies that the metric approaches the Minkowski metric at spatial infinity, i.e., $f, q, b, \omega \rightarrow 0$ asymptotically. In particular, the mass and the angular momentum can be read off from the components g_{tt} and $g_{t\varphi}$,

$$g_{tt} \xrightarrow{r \rightarrow \pm\infty} 1 \mp \frac{2GM_{\pm}}{r}, \quad g_{t\varphi} \xrightarrow{r \rightarrow \pm\infty} \frac{2GJ_{\pm}}{r} \sin^2 \theta.$$

Then, for the extraction of the global charges, one needs to study the behaviour of the metric functions at infinity,

$$f \approx \mp \frac{2\bar{M}_{\pm}}{x} + \dots, \quad \bar{\omega} \approx \frac{2\bar{J}_{\pm}}{x^3} + \dots,$$

where we have introduced the dimensionless quantities $\bar{M}_{\pm} \equiv m_s M_{\pm} / M_p^2$ [cf. Eq. (19)] and $\bar{J}_{\pm} \equiv (m_s / M_p)^2 J_{\pm}$ [cf. Eq. (17)] with $M_p = G^{-1/2}$ being the Planck mass. The ADM masses of the configuration \bar{M}_{\pm} and the angular momenta \bar{J}_{\pm} appearing in the above expressions may then be represented in the form

$$\bar{M}_{\pm} = \pm \frac{1}{2} \lim_{x \rightarrow \pm\infty} x^2 \partial_x f = \pm \frac{c_k}{8} \lim_{\bar{x} \rightarrow \pm 1} \frac{\partial_{\bar{x}} f}{1 - \bar{x}^2}, \quad \bar{J}_{\pm} = \frac{1}{2} \lim_{x \rightarrow \pm\infty} x^3 \bar{\omega} = \pm \frac{c_k^3}{2} \lim_{\bar{x} \rightarrow \pm 1} \frac{\bar{\omega}}{(1 - \bar{x}^2)^6}. \quad (13)$$

Our aim is to find globally regular solutions describing localized, finite-mass configurations embedded in an asymptotically flat spacetime. To do this, on account of the asymptotic behaviour given above, we impose appropriate boundary conditions for the metric functions at two spatial infinities ($x \rightarrow \pm\infty$) and on the z -axis ($\theta = 0$ and $\theta = \pi$). Namely, we take

$$\begin{aligned} f|_{x \rightarrow \pm\infty} &= q|_{x \rightarrow \pm\infty} = b|_{x \rightarrow \pm\infty} = \omega|_{x \rightarrow \pm\infty} = 0; \\ \frac{\partial f}{\partial \theta} \Big|_{\theta=0, \pi} &= \frac{\partial q}{\partial \theta} \Big|_{\theta=0, \pi} = b|_{\theta=0, \pi} = \frac{\partial \bar{\omega}}{\partial \theta} \Big|_{\theta=0, \pi} = 0. \end{aligned} \quad (14)$$

Note here that, in order to ensure the absence of a conical singularity, we must take $b|_{\theta=0, \pi} = 0$ (the elementary flatness condition).

In turn, for the matter fields, we take the following boundary conditions:

$$\begin{aligned} \bar{X}|_{x \rightarrow \pm\infty} &= \bar{Y}|_{x \rightarrow \pm\infty} = \bar{V}|_{x \rightarrow \pm\infty} = \bar{W}|_{x \rightarrow \pm\infty} = \bar{\phi}|_{x \rightarrow -\infty} = \bar{\sigma}|_{x \rightarrow \pm\infty} = 0, \quad \bar{\phi}|_{x \rightarrow +\infty} = \bar{\phi}_{+\infty}; \\ \frac{\partial \bar{X}}{\partial \theta} \Big|_{\theta=0} &= \frac{\partial \bar{V}}{\partial \theta} \Big|_{\theta=0} = \frac{\partial \bar{\phi}}{\partial \theta} \Big|_{\theta=0} = 0, \quad \bar{Y}|_{\theta=0} = \bar{W}|_{\theta=0} = \bar{\sigma}|_{\theta=0} = 0; \\ \frac{\partial \bar{Y}}{\partial \theta} \Big|_{\theta=\pi} &= \frac{\partial \bar{W}}{\partial \theta} \Big|_{\theta=\pi} = \frac{\partial \bar{\phi}}{\partial \theta} \Big|_{\theta=\pi} = 0, \quad \bar{X}|_{\theta=\pi} = \bar{V}|_{\theta=\pi} = \bar{\sigma}|_{\theta=\pi} = 0. \end{aligned} \quad (15)$$

B. Wormhole throat and angular momentum

We consider configurations possessing a nontrivial spacetime topology that are asymptotically flat and asymmetric with respect to the center $x = 0$. The most important geometrical characteristic of the configurations is their throat. Due to the asymmetry, the throat is located at the hypersurface $x \neq 0$, which represents a minimal surface. Then the equatorial radius of the throat is given by [11, 12, 14]

$$\bar{R}_e \equiv m_s R_e = \sqrt{-g_{\varphi\varphi}}|_{x=x_e, \theta=\pi/2} = e^{(q-f)/2} \sqrt{x^2 + x_0^2} \Big|_{x=x_e, \theta=\pi/2}, \quad (16)$$

where x_e is the value of the radial coordinate x for which a minimum of \bar{R}_e in the equatorial plane is located.

The total dimensionless angular momentum reads

$$\bar{J} \equiv (m_s/M_p)^2 J = -\frac{1}{2} \int_{-\infty}^{\infty} dx \int_0^{\pi} d\theta \bar{T}_{\varphi}^t e^{b-f+3q/2} (x^2 + x_0^2) \sin \theta, \quad (17)$$

where the dimensionless (t_{φ})-component of the energy-momentum tensor (6) is given by Eq. (A16). The occurrence of a nonzero angular momentum (17) is due to the presence in the system of a single spinor field possessing an intrinsic half-integer momentum. In turn, the numerical calculations indicate that the contribution coming from the electric and magnetic fields is equal to zero.

The conserved spinor charge associated with the Noether current is obtained using the expression for the spinor four-current j^{μ} [see after Eq. (5)] in the form

$$Q_{\psi} = \int j^t \sqrt{-g} dr d\theta d\varphi = \frac{1}{2} \left(\frac{M_p}{m_s} \right)^2 \int_{-\infty}^{\infty} dx \int_0^{\pi} d\theta e^{b+3(q-f)/2} (\bar{X}^2 + \bar{Y}^2 + \bar{V}^2 + \bar{W}^2) (x^2 + x_0^2) \sin \theta. \quad (18)$$

Note that there is a general relation for the angular momentum of a spinor field [30], leading to

$$J = m Q_{\psi}.$$

Our numerical results indicate that for all solutions $m = 1/2$, i.e., $m = M_{\psi}$, as it should be¹. Consequently, the solutions can be thought of as corresponding to minima of the total energy functional (the Komar mass)

$$\bar{M} \equiv m_s M/M_p^2 = \frac{1}{2} \int_{-\infty}^{\infty} dx \int_0^{\pi} d\theta (2\bar{T}_t^t - \bar{T}_{\mu}^{\mu}) e^{b-f+3q/2} (x^2 + x_0^2) \sin \theta \quad (19)$$

with fixed angular momentum.

C. Numerical method

We solve the set of mixed order partial differential equations (A2)-(A11) with the boundary conditions (14) and (15). In order to map the infinite range of the radial variable x to the finite interval, we introduce the compactified coordinate \bar{x} as

$$x = c_k \frac{\bar{x}}{(1 - \bar{x}^2)^2}, \quad (20)$$

which maps the infinite region $(-\infty; \infty)$ onto the finite interval $[-1; 1]$. Here c_k is a constant which is used to adjust the contraction of the grid. In our calculations, we typically take $c_k = 1$.

Technically, Eqs. (A2)-(A11) are discretized on some grid, and the resulting set of nonlinear algebraic equations is then solved by using a modified Newton method. The underlying linear system is solved with the Intel MKL PARDISO sparse direct solver [39] and the CESDSOL library². Typical mesh sizes include 400×400 points covering the integration region $-1 \leq \bar{x} \leq 1$ [given by the compact radial coordinate (20)] and $0 \leq \theta \leq \pi$. In all cases, the typical errors are of order of 10^{-4} . The package provides an iterative procedure to obtain an exact solution starting from some initial guess configuration. As such a configuration, we take a nonrotating system found in Ref. [29].

¹ Recall that we restrict our considerations to the case $M_{\psi} = 1/2$.

² Complex Equations-Simple Domain partial differential equations SOLver, a C++ package developed by I. Perapechka, see Refs. [30, 31].

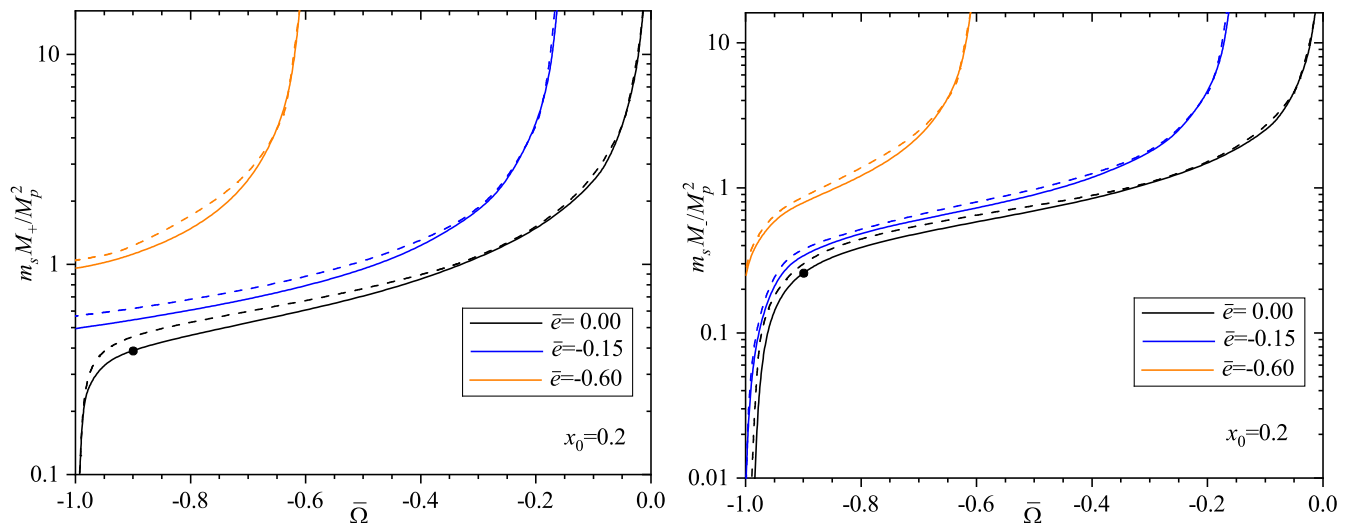


FIG. 1. The dimensionless total masses \bar{M}_\pm as functions of the parameter $\bar{\Omega}$ for neutral and charged spinor fields with different values of the coupling constant \bar{e} . The solid lines correspond to the rotating systems, while the dashed lines are for the nonrotating configurations. The bold dots correspond to the configurations for which the solutions are displayed in Fig. 6.

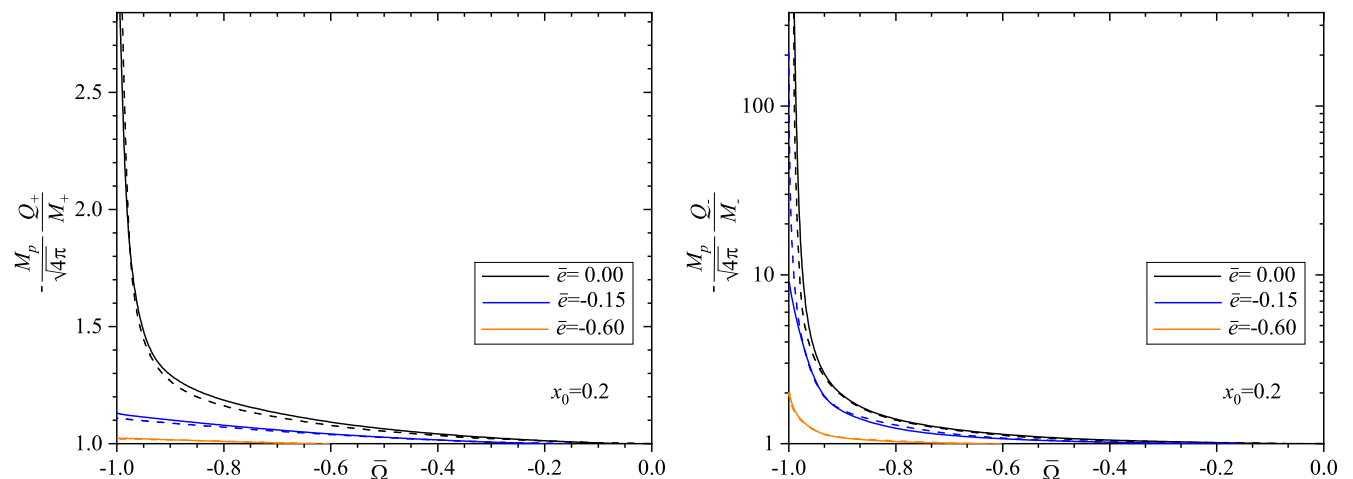


FIG. 2. The ratio of the charges of the configurations to their masses \bar{Q}_\pm/\bar{M}_\pm as a function of $\bar{\Omega}$ for different values of \bar{e} . The solid lines correspond to the rotating systems, while the dashed lines are for the nonrotating configurations.

For given values of three input parameters x_0 , $\bar{\Omega}$, and \bar{e} , we adjust the asymptotic value $\bar{\phi}_{+\infty}$ [see Eq. (11)] such that the constraint equation $d \equiv (E_x^x - E_\theta^\theta) = 0$ vanishes (to a given accuracy). For this purpose, we have introduced the L_2 norm of the constraint

$$D(\bar{\phi}_{+\infty}) = \left[\int_{-\infty}^{+\infty} dx \int_0^\pi d\theta d^2(x, \theta) \right]^{1/2}$$

and verified that the value of $D \sim 10^{-4} - 10^{-3}$, which is comparable with the L_2 norm of the solutions of the partial differential equations (A2)-(A11).

D. Results of numerical calculations

The search for finite-energy solutions to the set of equations (A2)-(A11) is performed by assigning different values of the free system parameters x_0 , $\bar{\Omega}$, and \bar{e} for which one can find regular solutions. Notice that since here we construct solutions for classical fields, the Noether charge Q_ψ calculated using (18) is some arbitrary number whose value in

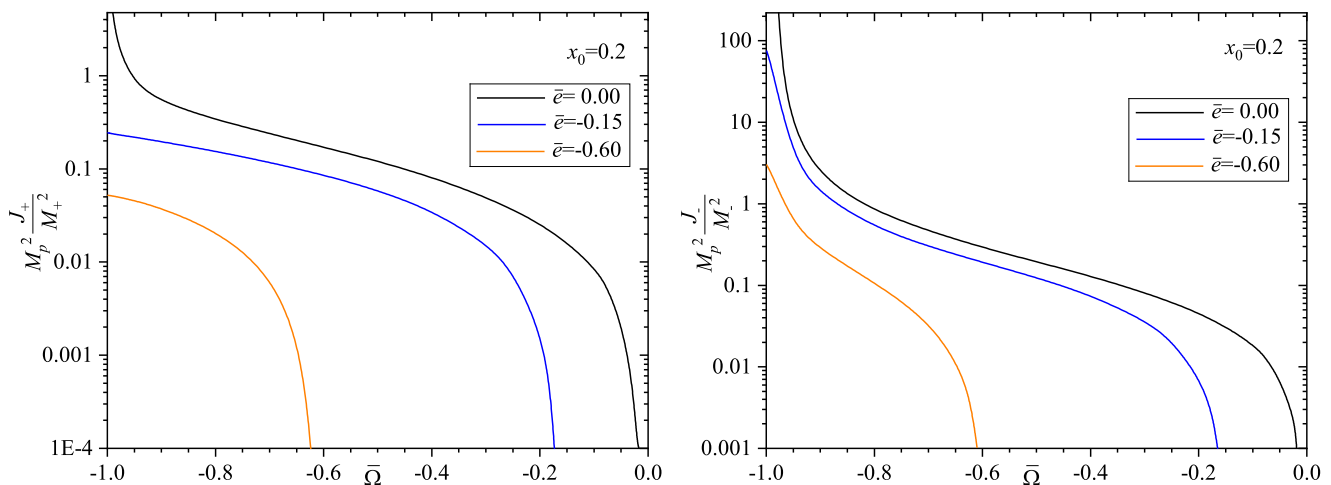


FIG. 3. The ratio of the angular momenta of the configurations to their masses $a_{*\pm} = \bar{J}_{\pm} / \bar{M}_{\pm}^2$ as a function of $\bar{\Omega}$ for different values of \bar{e} .

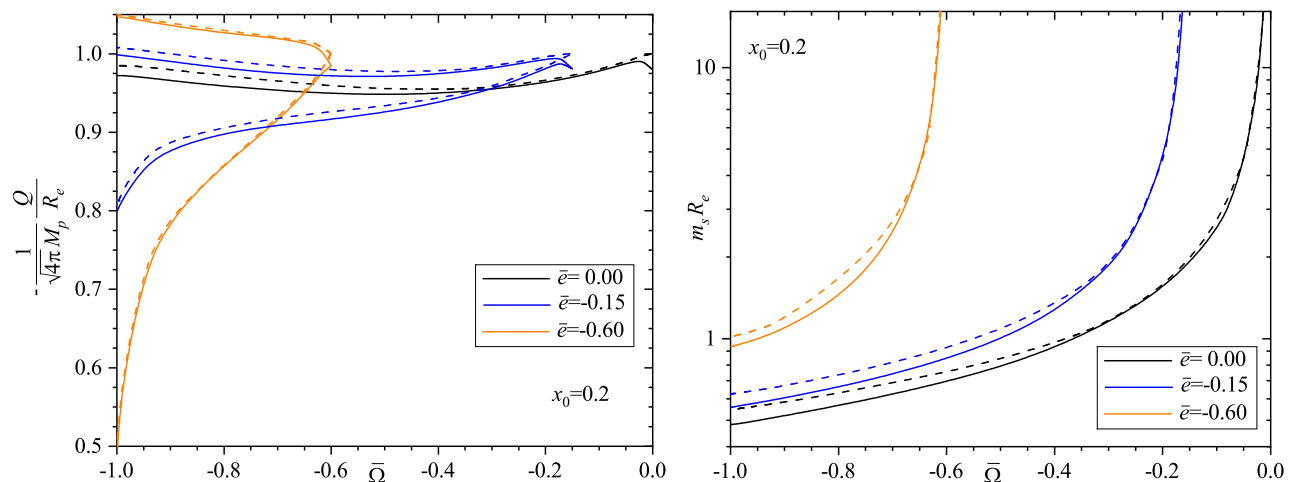


FIG. 4. The ratio of the charges of the configurations to the equatorial radius of their throat $\bar{Q}_{\pm} / \bar{R}_e$ (left panel) and the equatorial radius \bar{R}_e (right panel) as functions of $\bar{\Omega}$ for different values of \bar{e} . The solid lines correspond to the rotating systems, while the dashed lines are for the nonrotating configurations. For the systems with $\bar{e} = 0$, the charges \bar{Q}_+ and \bar{Q}_- are equal, $\bar{Q}_+ = \bar{Q}_- = \bar{Q}$. For the systems with $\bar{e} \neq 0$, there are turning points located at $\bar{\Omega} = \bar{\Omega}_{\text{crit}}$: the upper parts of the curves correspond to the charge \bar{Q}_+ , while the lower parts are for the charge \bar{Q}_- .

general is determined by the specific values of the input parameters x_0 , $\bar{\Omega}$, and \bar{e} , as well as by the mass of the spinor field m_s . However, if one goes beyond the classical treatment of the fields and imposes the quantum nature of fermions, this requires that $Q_{\psi} = 1$ – the one-particle condition. Since in the present paper we are interested precisely in one-particle solutions (see Introduction), all results given below correspond to such solutions, i.e., we always impose the normalization condition $Q_{\psi} = 1$. This results in the fact that each of sequences of solutions for a fixed x_0 shown in the figures below corresponds to configurations with constant $Q_{\psi} = 1$ and varying mass of the spinor field m_s (that is, the curves correspond to sequences of solutions of different models).

The corresponding results of numerical calculations are shown in Fig. 1, where the dependencies of the masses \bar{M}_+ and \bar{M}_- [calculated using the asymptotic expression given by Eq. (13)] on the frequency $\bar{\Omega}$ for different values of the coupling constant \bar{e} are given. [Note here that the sum of the masses \bar{M}_+ and \bar{M}_- yields a total mass calculated using the Komar mass integral (19).] For a direct comparison, this figure also shows the corresponding results for nonrotating wormholes obtained in our previous work [29] (notice that in that paper we used another sign for the coupling constant e). It is seen from the comparison that a qualitative behaviour of the mass curves of the rotating configurations remains the same as that of the nonrotating systems: as \bar{e} increases (modulus), the mass curves shift to the left of the mass curve for the uncoupled case. In this case when $\bar{\Omega} \rightarrow -1$ the configurations with $\bar{e} \neq 0$, in contrast to the systems with $\bar{e} = 0$, may already have the masses \bar{M}_{\pm} which differ considerably from 0; also, the

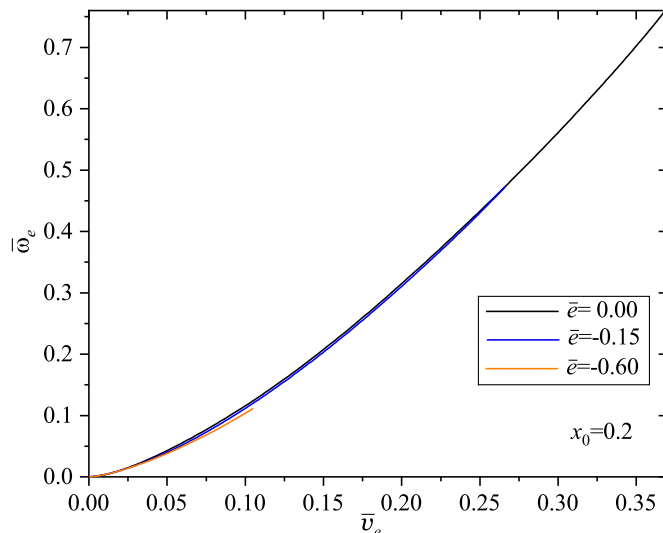


FIG. 5. The angular velocity of the throat, $\bar{\omega}_e$, versus the rotational velocity of the throat, \bar{v}_e , in the equatorial plane. The graphs for $\bar{e} = 0$ and $\bar{e} = -0.15$ practically coincide.

masses gradually increase with increasing $\bar{\Omega}$ and the magnitude of the coupling constant. As a result, for every value of \bar{e} , there is some critical value $\bar{\Omega}_{\text{crit}} \approx \bar{e}$ for which a fast increase in mass occurs (the mass demonstrates a divergent behaviour). In this case the behaviour of other characteristics of the systems under consideration remains similar to that of the case with no rotation: (i) the masses \bar{M}_+ and \bar{M}_- become equal; (ii) the metric function $g_{tt} \equiv e^f \rightarrow 0$ and the dimensionless Kretschmann scalar $\bar{K} \equiv K/m_s^4 = \bar{R}_{\alpha\beta\mu\nu}\bar{R}^{\alpha\beta\mu\nu}$ is practically equal to zero throughout all of space; (iii) for all the solutions, the ratio $-\bar{Q}_{\pm}/\bar{M}_{\pm} \rightarrow 1$ from above, as demonstrated in Fig. 2. Notice also that it is evident from the behaviour of the mass curves that, as in the case with no rotation [29], when $\bar{e} \rightarrow -1$, it is expected that the corresponding mass curve will degenerate. Thus the type of solutions considered in the present paper is probably only possible in the range $-1 \leq \bar{e} \leq 0$.

In turn, as shown in Fig. 3, the dimensionless ratio $a_{*\pm} = \bar{J}_{\pm}/\bar{M}_{\pm}^2$ varies within wide limits from $a_{*\pm} \approx 0$ to $a_{*-} \gg 1$, in contrast to Kerr-Newman black holes for which a_* ranges from 0 to 1. It is seen from Figs. 2 and 3 that for the configurations with $\bar{e} = 0$ located to the left of the center the ratios \bar{Q}_-/\bar{M}_- and \bar{J}_-/\bar{M}_-^2 demonstrate a fast increase when $\bar{\Omega} \rightarrow -1$. This is because, in this limit, the mass of the configurations under consideration goes to zero (see Fig. 1), and can even be negative, as demonstrated in Ref. [29] for nonrotating systems and in Ref. [40] for rotating configurations.

The left panel of Fig. 4 shows the ratio of the charge of the system [calculated using Eq. (12)] to the equatorial radius of the throat [calculated using Eq. (16)]. It is seen from this figure that the presence of rotation does not also result in a considerable qualitative change in the behaviour of these curves as compared with the curves for the nonrotating systems, except the vicinity of the points where $\bar{\Omega} \rightarrow \bar{\Omega}_{\text{crit}}$. Namely, when the coupling constant \bar{e} is zero, the ratio depends only slightly on the spinor frequency $\bar{\Omega}$, and is always of the order of 1, both for the rotating and nonrotating configurations. However, when $\bar{e} \neq 0$ the situation changes drastically: as the coupling constant increases in magnitude, the ratio $-\bar{Q}_+/\bar{R}_e$ becomes increasingly large as $\bar{\Omega}$ decreases, whereas the ratio $-\bar{Q}_-/\bar{R}_e$ becomes smaller and smaller. On the other hand, as $\bar{\Omega} \rightarrow \bar{\Omega}_{\text{crit}} \approx \bar{e}$, we have $-\bar{Q}_{\pm}/\bar{R}_e \rightarrow 1$ for the nonrotating systems, whereas for the rotating systems this ratio is always smaller than 1. In turn, the right panel of Fig. 4 shows that the equatorial radius of the throat \bar{R}_e of nonrotating systems is always slightly greater than that of the rotating configurations.

Note here that, taking into account the comparison of the behaviour of the masses, charges, and equatorial radii of the rotating systems considered here and nonrotating configurations of Ref. [29] given in Figs. 1, 2, and 4 for the case of the throat parameter $x_0 = 0.2$, it is evident that the rotation does not bring about any considerable qualitative changes. In this connection, one may expect that for other values of the throat parameter x_0 the inclusion of rotation will not change significantly a qualitative behaviour of the above characteristics as well. The corresponding results can be found in Ref. [29] where nonrotating systems with the values of x_0 lying in the range from 0.03 to 5 were considered.

Fig. 5 shows the dependence of the angular velocity of the throat $\bar{\omega}_e \equiv \bar{\omega}(x_e)$ on the rotational velocity of the throat in the equatorial plane, $\bar{v}_e = \bar{R}_e \bar{\omega}_e$. It is seen from this figure that the rotational velocity is always smaller than the velocity of light (equal to 1), and a maximum value of \bar{v}_e decreases with increasing the coupling constant $|\bar{e}|$. The

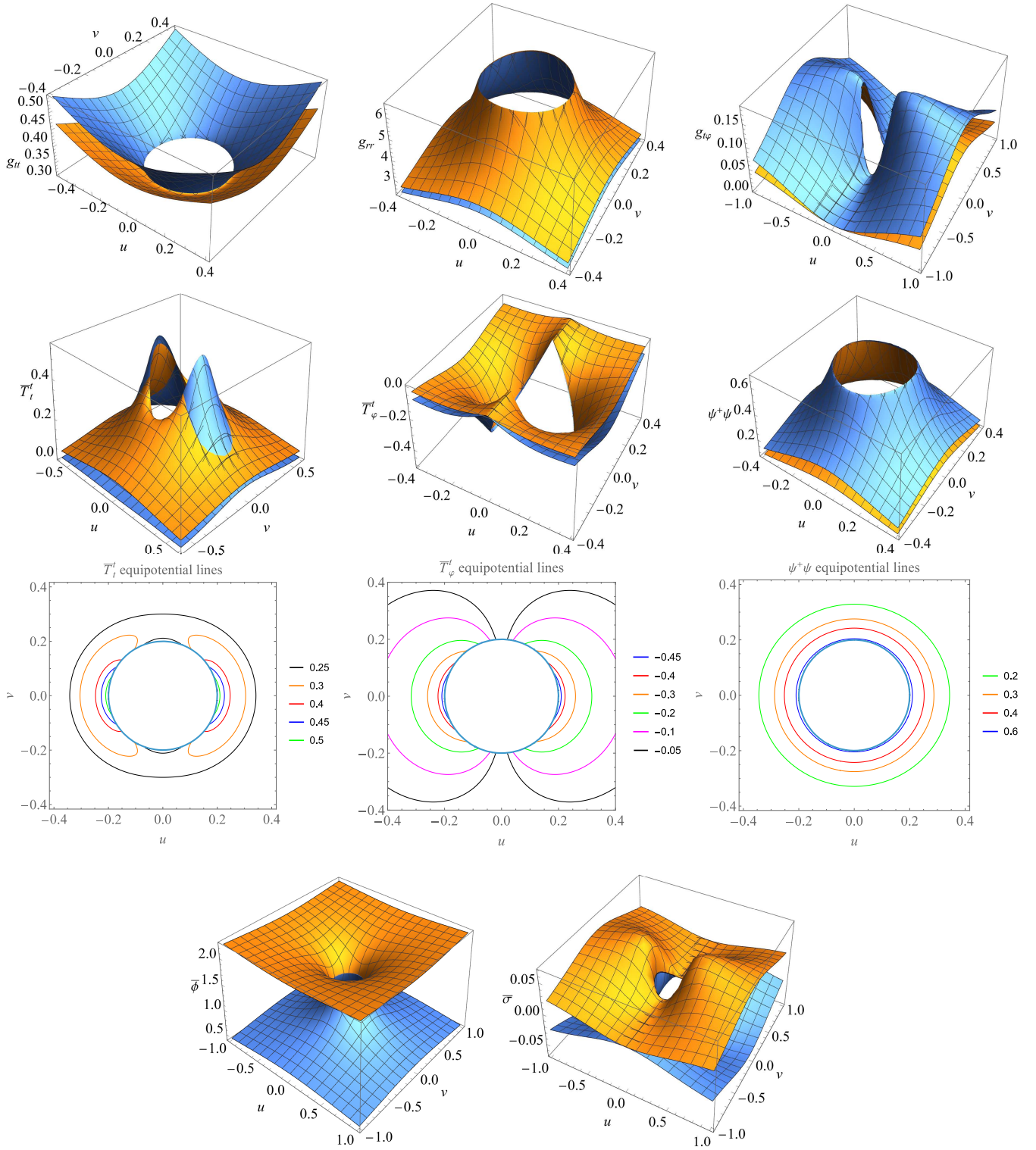


FIG. 6. Solutions for the system with the coupling constant $\bar{e} = 0$, the throat parameter $x_0 = 0.2$, and the spinor frequency $\bar{\Omega} = -0.9$ near the center of the configuration. The plots are made in a meridional plane $\varphi = \text{const.}$ spanned by the coordinates $u = \sqrt{x^2 + x_0^2} \sin \theta$ and $v = \sqrt{x^2 + x_0^2} \cos \theta$. The different rows show: the metric components g_{tt}, g_{rr} , and $g_{t\varphi}$; the total energy density \bar{T}_t^t , the angular momentum density \bar{T}_φ^t (physical component), and the spinor field density $\psi^\dagger \psi$; equipotential lines for the energy density, the angular momentum density, and the spinor field density in the subspace with $x > 0$; electric, $\bar{\phi}$, and magnetic, $\bar{\sigma}$, potentials. The yellow surfaces correspond to the solutions in the subspace with $x > 0$, while the blue ones are for the solutions in the subspace with $x < 0$. The throat in the equatorial plane ($\theta = \pi/2$) is located in the subspace with $x < 0$ at $u_e \approx 0.2$.

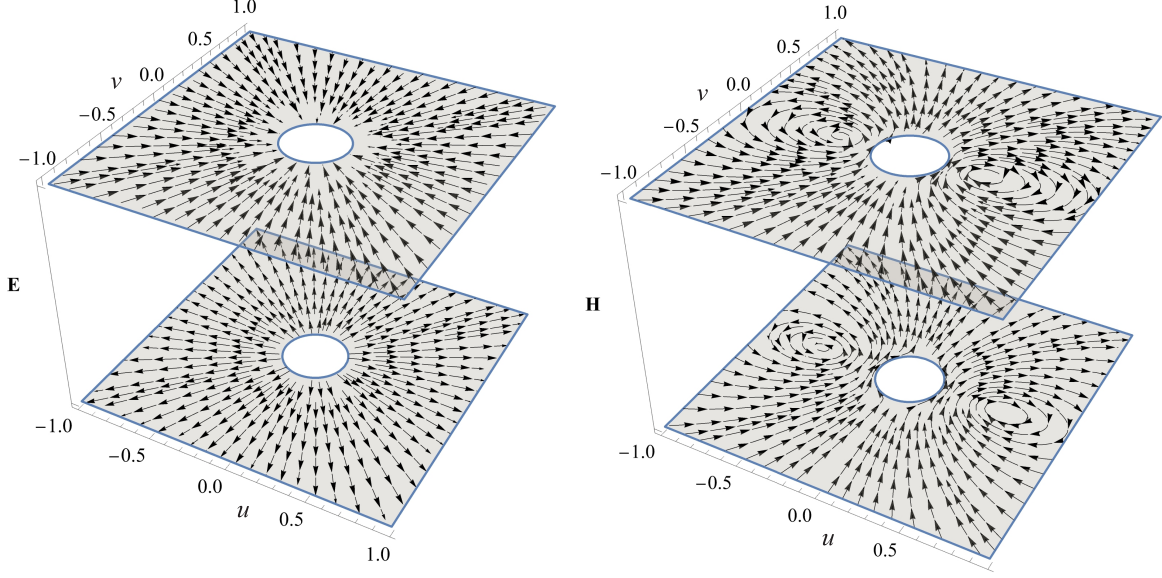


FIG. 7. Lines of force of the dimensionless electric, $\bar{\mathbf{E}} \equiv \sqrt{4\pi G}/m_s \mathbf{E}$, and magnetic, $\bar{\mathbf{H}} \equiv \sqrt{4\pi G}/m_s \mathbf{H}$, fields. The top plots correspond to the subspace with $x > 0$, while the bottom plots are for the subspace with $x < 0$.

leftmost points of the curves (when $\bar{v}_e \rightarrow 0$) correspond to the systems with $\bar{\Omega} \rightarrow \bar{\Omega}_{\text{crit}} \approx \bar{e}$, while the rightmost points are for the configurations with $\bar{\Omega} \rightarrow -1$.

The typical spatial distributions of the field functions are exemplified by Figs. 6 and 7 for the case of the system with the uncoupled spinor field ($\bar{e} = 0$). The plots are made in a meridional plane $\varphi = \text{const.}$ spanned by the coordinates $u = \sqrt{x^2 + x_0^2} \sin \theta$ and $v = \sqrt{x^2 + x_0^2} \cos \theta$. Such coordinates imply that the whole space is divided into two subspaces located at $x > 0$ and $x < 0$, and they are joined together along a circle with radius x_0 . As explicitly clear from the graphs shown in Fig. 6, there is an asymmetry of the solutions with respect to the reflection of the radial coordinate, $x \rightarrow -x$, whereas the solutions are symmetric with respect to the equatorial plane $\theta = \pi/2$. In turn, from the graphs of equipotential lines of the energy density \bar{T}_t^t , one can clearly see the configuration oblateness along the rotation axis v (see the line 0.25). Also, from the graphs for the electric, \mathbf{E} , and magnetic, \mathbf{H} , field strengths calculated using Eq. (10) and shown in Fig. 7, it is seen that the electric lines of force enter the throat from the subspace with $x > 0$ and exit to the subspace with $x < 0$. In turn, the magnetic field demonstrates a behaviour typical of an axially symmetric dipole field sourced by the current associated with the spinor field and given by the right-hand side of Eq. (5).

Let us now demonstrate the influence of the magnitude of the throat parameter x_0 on the geometry of the wormhole. To do so, consider the shape of wormholes rotating with different rotational velocities, but having equal throat radii \bar{R}_e . For this purpose, we employ the embedding diagram, using which one can visualize the wormhole metric at fixed t in the equatorial plane $\theta = \pi/2$. Namely, the wormhole metric can be isometrically embedded in Euclidean space as follows:

$$ds^2 = e^{q-f+b} dr^2 + e^{q-f} h d\varphi^2 = d\rho^2 + \rho^2 d\varphi^2 + dz^2,$$

where $\rho = \rho(r)$ and $z = z(r)$. Hence it follows that

$$\left(\frac{d\rho}{dr}\right)^2 + \left(\frac{dz}{dr}\right)^2 = e^{q-f+b}, \quad \rho^2 = e^{q-f} (r^2 + r_0^2),$$

and this enables one to find the corresponding dependence $z(r)$. Then, using the above parametric dependencies $\rho = \rho(r)$ and $z = z(r)$, we show in Fig. 8 the embedding diagrams for the wormholes supported by a neutral spinor field ($\bar{e} = 0$) with fixed equatorial throat radius $\bar{R}_e \approx 1.5$ spinning with the rotational velocities $\bar{v}_e = 0.04$ (the case of $x_0 = 0.2, \bar{\Omega} = -0.2$) and $\bar{v}_e = 0.32$ (the case of $x_0 = 1, \bar{\Omega} = -0.9$). Hence we see that to obtain the required fixed radius $\bar{R}_e \approx 1.5$ the configuration with $x_0 = 1$ must rotate with the rotational velocity which is eight times the velocity of the system with $x_0 = 0.2$. This, of course, has the result that the shape of the wormhole becomes squeezed down along the rotation axis z' , as demonstrated in Fig. 8.

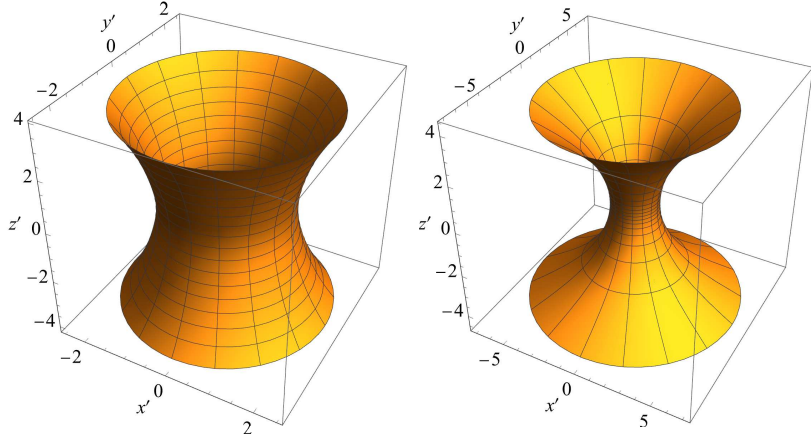


FIG. 8. Rotating wormholes at fixed equatorial throat radius $\bar{R}_e \approx 1.5$ spinning with the rotational velocities $\bar{v}_e = 0.04$ (when $x_0 = 0.2$) and $\bar{v}_e = 0.32$ (when $x_0 = 1$). The plots are made in Cartesian coordinates $\{x', y', z'\}$. The regions for $z' > 0$ correspond to the subspace with dimensionless radial coordinate $x > 0$, while the regions for $z' < 0$ correspond to the subspace with $x < 0$.

To conclude this section, let us now determine the polar circumferential radius of the throat. To do this, it is necessary to find a dependence of a coordinate radius of the throat r_{th} on θ . For this purpose one has to construct an embedding diagram that describes the intrinsic geometry of the throat surface [i.e., the spacetime slice with $t = \text{const.}$ and $r = r_{\text{th}}(\theta)$]. To do so, it is necessary to embed the throat surface in a flat three-dimensional space [41]. This can be done as follows: we parameterize the surface of the throat by the coordinates $\{r_{\text{th}}(\theta), \theta, \varphi\}$. Then the line element on the throat surface induced by the four-dimensional metric (7) is

$$ds_{\text{th}}^2 = e^{q_{\text{th}} - f_{\text{th}}} \left\{ e^{b_{\text{th}}} \left[(\partial_{\theta} r_{\text{th}})^2 + h_{\text{th}} \right] d\theta^2 + h_{\text{th}} \sin^2 \theta d\varphi^2 \right\}, \quad (21)$$

where the index “th” corresponds to the surface of the throat where the metric functions are given [for example, $f_{\text{th}} \equiv f(r_{\text{th}}(\theta), \theta)$] and $h_{\text{th}} = r_{\text{th}}^2 + r_0^2$. The area of the surface is now given by the integral of the square root of the determinant of the metric tensor [12]

$$A_{s_{\text{th}}} = \int L_{s_{\text{th}}} d\theta d\varphi \quad (22)$$

with

$$L_{s_{\text{th}}} = \sqrt{(\partial_{\theta} r_{\text{th}})^2 + h_{\text{th}}} \sqrt{h_{\text{th}}} \sin \theta e^{q_{\text{th}} - f_{\text{th}} + b_{\text{th}}/2}.$$

The function $r_{\text{th}}(\theta)$ is determined as the solution of the corresponding Euler-Lagrange equation that minimizes the magnitude of the area of the surface from Eq. (22) (for details, see Ref. [12]). This Euler-Lagrange equation is solved with the boundary condition $\partial_{\theta} r_{\text{th}}|_{\theta=0} = 0$, which ensures the regularity.

In order to determine the polar radius of the configuration under consideration, it is convenient to employ cylindrical coordinates $\{\rho, z, \varphi\}$ for the flat space. Using the metric (21), we then have the following formulas [41]:

$$\rho(\theta) = e^{(q_{\text{th}} - f_{\text{th}})/2} \sqrt{h_{\text{th}}} \sin \theta, \quad z(\theta) = \int_{\theta}^{\pi/2} d\theta' \left\{ e^{q_{\text{th}} - f_{\text{th}} + b_{\text{th}}} \left[\left(\frac{dr_{\text{th}}}{d\theta'} \right)^2 + h_{\text{th}} \right] - \left(\frac{d\rho}{d\theta'} \right)^2 \right\}^{1/2}.$$

The equatorial and polar radii of the embedded surface are then given by

$$R_e = \rho \left(\theta = \frac{\pi}{2} \right) = e^{(q_{\text{th}} - f_{\text{th}})/2} \sqrt{h_{\text{th}}} \Big|_{\theta=\pi/2}, \quad [\text{cf. Eq. (16)}]$$

$$R_p = z(\theta = 0) = \int_0^{\pi/2} d\theta' \left\{ e^{q_{\text{th}} - f_{\text{th}} + b_{\text{th}}} \left[\left(\frac{dr_{\text{th}}}{d\theta'} \right)^2 + h_{\text{th}} \right] - \left(\frac{d\rho}{d\theta'} \right)^2 \right\}^{1/2}.$$

Using these formulas, we have found that the maximum value of the ratio $R_e/R_p \approx 1.02$ is for the system with $\bar{v} = 0$ when $\bar{\Omega} \rightarrow -1$. Thus, for all configurations with $x_0 = 0.2$ considered in the present paper the rotation brings about only a small oblateness along the rotation axis.

IV. CONCLUSIONS AND DISCUSSION

In the present paper we have studied rotating, axially symmetric and asymptotically flat wormhole solutions supported by a complex non-phantom spinor field and electric and magnetic fields within Einstein gravity. The resulting wormholes connect two identical Minkowski spacetimes. Despite the fact that the spinor field is a non-phantom field, it ensures the violation of the energy conditions, and correspondingly the possibility for the systems under consideration to have a nontrivial wormhole topology. The complex spinor field has an explicit dependence on time and azimuthal angle, while still retaining a stationary axially symmetric metric. In turn, the $U(1)$ invariance of the model gives rise to a conserved current and an associated conserved Noether charge.

Analogous to Dirac stars, the harmonic time dependence includes a spinor frequency $\bar{\Omega}$, whereas the angular dependence involves an azimuthal number M_ψ , and the angular momentum turns out to be proportional to the Noether charge with a proportionality coefficient M_ψ . However, in other aspects, the Dirac stars and wormholes supported by the spinor field differ considerably. In particular, for the Dirac stars, the dependencies of their mass on the spinor frequency have a typical spiral-like form, both for nonrotating systems [42] and for configurations with rotation [30, 31]. At the same time, it is typical of the systems with a nontrivial spacetime topology that this dependence varies monotonically both for the nonrotating [29] and rotating configurations considered here. Also, regular solutions for the Dirac stars do exist only in a restricted range of frequencies $\bar{\Omega} > \bar{\Omega}_{\min}$, whereas the wormhole solutions are present in all the frequency range $-1 \leq \bar{\Omega} < 0$.

The studies indicate that for the values of the system parameters considered in the present paper the main physical characteristics of the rotating systems are comparable to those of the nonrotating configurations of Ref. [29]. Let us enumerate the most interesting features of the configurations under consideration:

- (i) In the case of an uncharged spinor field ($\bar{e} = 0$), there is a qualitatively similar behaviour of the dependencies of the ADM masses on the spinor frequency $\bar{\Omega}$: as $\bar{\Omega} \rightarrow -1$, the masses are approximately equal to zero; as $\bar{\Omega} \rightarrow -0$, the masses increase according to the law $M_\pm \sim |\bar{\Omega}|^{-1}$. In this case, as $\bar{\Omega}$ increases from -1 to 0, the masses increase smoothly (with no turning points), unlike the Dirac stars [30, 31].
- (ii) In the case of a charged spinor field ($\bar{e} \neq 0$), the behaviour of the mass curves resembles in general the case of the systems with $\bar{e} = 0$: here there is also some critical value $\bar{\Omega}_{\text{crit}} \approx \bar{e}$ for which, as in the case with $\bar{e} = 0$, there is a fast increase in mass which demonstrates a divergent behaviour as $\bar{\Omega} \rightarrow \bar{\Omega}_{\text{crit}}$. However, unlike the systems with $\bar{e} = 0$, as $\bar{\Omega} \rightarrow -1$, the configurations with $\bar{e} \neq 0$ may already have a mass which is considerably different from zero and gradually increases with increasing $\bar{\Omega}$ and the magnitude of the coupling constant.
- (iii) All the solutions considered are asymmetric with respect to the reflection of the radial coordinate, $x \rightarrow -x$, whereas the solutions are symmetric with respect to the equatorial plane $\theta = \pi/2$. The rotation of the spinor field drags the throat and the spacetime along, allowing for asymmetric rotating wormholes.
- (iv) An increase in the magnitude of the throat parameter x_0 for a fixed value of the equatorial throat radius results in the growth of the rotational velocity of the throat.

Thus we have obtained a wormhole having the mass, angular momentum, electric and magnetic fields. The electric field enters the wormhole from one asymptotically flat spacetime with the radial coordinate $r > 0$ and exits to another asymptotically flat spacetime with $r < 0$. This means that the solution obtained incarnates Wheeler's idea of "mass without mass" and "charge without charge" [43]; moreover, the system possesses a nonzero angular momentum. Such solution can be regarded as a model of a *classical charge possessing a spin*. However, it should be emphasised that such a wormhole cannot be naively used as a model of an electron, since in general the wormhole has different charges to the left and to the right of the throat, whose magnitudes depend on the value of the system parameters e, Ω , and r_0 and are not equal to the charge of an electron (at least one of them), though it has the total angular moment 1/2 owing to the presence of the spinor field. In this connection we may also mention another approaches in constructing a nonperturbative model of an electron interacting with gravity, see, e.g., Ref. [44] and references therein.

ACKNOWLEDGEMENTS

We gratefully acknowledge support provided by the program No. AP26195069 (Bound states in Maxwell, Yang-Mills, Proca theories with and without gravity in the presence of spinor fields) of the Committee of Science of the Ministry of Science and Higher Education of the Republic of Kazakhstan.

Appendix A: Field equations

For performing numerical calculations, we introduce the following dimensionless variables and parameters:

$$\begin{aligned} x &= m_s r, \quad (\bar{\Omega}, \bar{\omega}) = (\Omega, \omega)/m_s, \quad (\bar{X}, \bar{Y}, \bar{V}, \bar{W}) = \sqrt{\frac{4\pi G}{m_s}}(X, Y, V, W), \\ \bar{\phi} &= \sqrt{4\pi G}\phi, \quad \bar{\sigma} = \sqrt{4\pi G}m_s\sigma, \quad \bar{e} = \frac{e}{\sqrt{4\pi G}m_s}. \end{aligned} \quad (\text{A1})$$

Then the Einstein field equations (2) yield the following set of coupled nonlinear elliptic partial differential equations:

$$f_{xx} - e^{-2f+q} \sin^2 \theta (h\bar{\omega}_x^2 + \bar{\omega}_\theta^2) + \left(\frac{2x}{h} + \frac{1}{2}q_x\right) f_x + \frac{f_{\theta\theta}}{h} + \frac{1}{2h} (2 \cot \theta + q_\theta) f_\theta = \bar{T}_t^t - \bar{T}_x^x - \bar{T}_\theta^\theta - \bar{T}_\varphi^\varphi + 2\bar{\omega}\bar{T}_\varphi^t, \quad (\text{A2})$$

$$q_{xx} + \frac{1}{2}q_x^2 + \frac{3x}{h}q_x + \frac{1}{h} \left(q_{\theta\theta} + \frac{1}{2}q_\theta^2 + 2 \cot \theta q_\theta\right) = \bar{T}_x^x + \bar{T}_\theta^\theta, \quad (\text{A3})$$

$$\begin{aligned} b_{xx} - \frac{3}{2}e^{-2f+q} \sin^2 \theta (h\bar{\omega}_x^2 + \bar{\omega}_\theta^2) + \frac{1}{2} (f_x^2 - q_x^2) + \frac{1}{h} \left[b_{\theta\theta} + x(b_x - 2q_x) + \frac{1}{2} (f_\theta^2 - q_\theta^2) - 2 \cot \theta q_\theta - \frac{2x^2}{h} + 2\right] \\ = \bar{T}_\varphi^\varphi - \bar{T}_x^x - \bar{T}_\theta^\theta - \bar{\omega}\bar{T}_\varphi^t, \end{aligned} \quad (\text{A4})$$

$$\bar{\omega}_{xx} + \left(\frac{4x}{h} - 2f_x + \frac{3}{2}q_x\right) \bar{\omega}_x + \frac{1}{h} \left[\bar{\omega}_{\theta\theta} + \left(3 \cot \theta - 2f_\theta + \frac{3}{2}q_\theta\right) \bar{\omega}_\theta\right] = \bar{T}_\varphi^t. \quad (\text{A5})$$

The Maxwell equations (5) take the form

$$\begin{aligned} \bar{\phi}_{xx} + \frac{\bar{\phi}_{\theta\theta}}{h} + e^{-2f+q} \bar{\omega} \sin^2 \theta [\bar{\omega}_\theta \bar{\phi}_\theta + h\bar{\omega}_x \bar{\phi}_x + \bar{\omega} (\bar{\omega}_\theta \bar{\sigma}_\theta + h\bar{\omega}_x \bar{\sigma}_x)] \\ + \frac{1}{2h} \left\{ 2\bar{\omega}_\theta \bar{\sigma}_\theta + (2 \cot \theta - 2f_\theta + q_\theta) \bar{\phi}_\theta + 2h\bar{\omega}_x \bar{\sigma}_x + 2\bar{\omega} [(2 \cot \theta - 2f_\theta + q_\theta) \bar{\sigma}_\theta + (2x + h[-2f_x + q_x]) \bar{\sigma}_x] \right. \\ \left. + [4x + h(-2f_x + q_x)] \bar{\phi}_x \right\} + \bar{e} e^{-3f/2+q} \left(e^f U_1 - 2e^{q/2} U_3 \sqrt{h} \bar{\omega} \sin \theta \right) = 0, \end{aligned} \quad (\text{A6})$$

$$\begin{aligned} \bar{\sigma}_{xx} + \frac{\bar{\sigma}_{\theta\theta}}{h} - e^{-2f+q} \sin^2 \theta [\bar{\omega}_\theta \bar{\phi}_\theta + h\bar{\omega}_x \bar{\phi}_x + \bar{\omega} (\bar{\omega}_\theta \bar{\sigma}_\theta + h\bar{\omega}_x \bar{\sigma}_x)] - \frac{1}{2h} [(2 \cot \theta - 2f_\theta + q_\theta) \bar{\sigma}_\theta + hq_x \bar{\sigma}_x] \\ + f_x \bar{\sigma}_x + 2\bar{e} e^{-3f/2+3q/2} \sqrt{h} \sin \theta U_3 = 0. \end{aligned} \quad (\text{A7})$$

The Dirac equations (3) are

$$\begin{aligned} \bar{X}_x + \frac{1}{4} \left(\frac{4x}{h} + b_x - f_x + 2q_x\right) \bar{X} - \frac{1}{\sqrt{h}} \bar{W}_\theta + \frac{1}{4} \left\{ e^{-f+q/2} \bar{V} \left[-2e^{b/2} \left(-\bar{\omega} [1 + 2\bar{e}\bar{\sigma}] + 2 \left[e^{f/2} + \bar{\Omega} - \bar{e}\bar{\phi} \right] \right) + \sin \theta \bar{\omega}_\theta \right] \right. \\ \left. - \frac{1}{\sqrt{h}} \left[2 \cot \theta + 2e^{b/2} \csc \theta (1 + 2\bar{e}\bar{\sigma}) + b_\theta - f_\theta + 2q_\theta \right] \bar{W} - e^{-f+q/2} \sqrt{h} \sin \theta \bar{Y} \bar{\omega}_x \right\} = 0, \end{aligned} \quad (\text{A8})$$

$$\begin{aligned} \bar{Y}_x + \frac{1}{4} \left(\frac{4x}{h} + b_x - f_x + 2q_x\right) \bar{Y} - \frac{1}{\sqrt{h}} \bar{V}_\theta + \frac{1}{4} \left\{ e^{-f+q/2} \bar{W} \left[-2e^{b/2} \left(\bar{\omega} [1 + 2\bar{e}\bar{\sigma}] + 2 \left[e^{f/2} - \bar{\Omega} + \bar{e}\bar{\phi} \right] \right) + \sin \theta \bar{\omega}_\theta \right] \right. \\ \left. - \frac{1}{\sqrt{h}} \left[2 \cot \theta - 2e^{b/2} \csc \theta (1 + 2\bar{e}\bar{\sigma}) + b_\theta - f_\theta + 2q_\theta \right] \bar{V} - e^{-f+q/2} \sqrt{h} \sin \theta \bar{X} \bar{\omega}_x \right\} = 0, \end{aligned} \quad (\text{A9})$$

$$\begin{aligned} \bar{V}_x + \frac{1}{4} \left(\frac{4x}{h} + b_x - f_x + 2q_x\right) \bar{V} + \frac{1}{\sqrt{h}} \bar{Y}_\theta + \frac{1}{4} \left\{ e^{-f+q/2} \bar{X} \left[-2e^{b/2} \left(\bar{\omega} [1 + 2\bar{e}\bar{\sigma}] + 2 \left[e^{f/2} - \bar{\Omega} + \bar{e}\bar{\phi} \right] \right) - \sin \theta \bar{\omega}_\theta \right] \right. \\ \left. + \frac{1}{\sqrt{h}} \left[2 \cot \theta + 2e^{b/2} \csc \theta (1 + 2\bar{e}\bar{\sigma}) + b_\theta - f_\theta + 2q_\theta \right] \bar{Y} - e^{-f+q/2} \sqrt{h} \sin \theta \bar{W} \bar{\omega}_x \right\} = 0, \end{aligned} \quad (\text{A10})$$

$$\begin{aligned} \bar{W}_x + \frac{1}{4} \left(\frac{4x}{h} + b_x - f_x + 2q_x\right) \bar{W} + \frac{1}{\sqrt{h}} \bar{X}_\theta + \frac{1}{4} \left\{ e^{-f+q/2} \bar{Y} \left[-2e^{b/2} \left(-\bar{\omega} [1 + 2\bar{e}\bar{\sigma}] + 2 \left[e^{f/2} + \bar{\Omega} - \bar{e}\bar{\phi} \right] \right) - \sin \theta \bar{\omega}_\theta \right] \right. \\ \left. + \frac{1}{\sqrt{h}} \left[2 \cot \theta - 2e^{b/2} \csc \theta (1 + 2\bar{e}\bar{\sigma}) + b_\theta - f_\theta + 2q_\theta \right] \bar{X} - e^{-f+q/2} \sqrt{h} \sin \theta \bar{V} \bar{\omega}_x \right\} = 0. \end{aligned} \quad (\text{A11})$$

In the above equations, the lower indices on the metric and field functions denote differentiation with respect to the corresponding coordinate and the dimensionless components of the energy-momentum tensor (6) appearing in the

right-hand sides of Eqs. (A2)-(A5) are

$$\begin{aligned} \bar{T}_t^t \equiv \frac{4\pi G}{m_s^2} T_t^t &= \frac{1}{8h^2} e^{-b-3f/2-2q} \left\{ 4e^{b+5q/2} U_3 h^{5/2} \sin \theta \bar{\omega} [-2\bar{\Omega} + \bar{\omega} + 2\bar{e} (\bar{\phi} + \bar{\sigma}\bar{\omega})] + 4e^{7f/2} \csc^2 \theta (\bar{\sigma}_\theta^2 + h\bar{\sigma}_x^2) \right. \\ &\quad - 4e^{3f/2+q} h [\bar{\omega}^2 (\bar{\sigma}_\theta^2 + h\bar{\sigma}_x^2) - h\bar{\phi}_x^2 - \bar{\phi}_\theta^2] + e^{b/2+f+2q} h^{3/2} \left\{ -4U_4 x \sin \theta \bar{\omega} \right. \\ &\quad + \sqrt{h} [-2e^{b/2} U_1 (-4\bar{\Omega} + \bar{\omega} + 2\bar{e} [2\bar{\phi} + \bar{\sigma}\bar{\omega}]) + U_2 \bar{\omega} (-2 \cos \theta + \sin \theta [2f_\theta - q_\theta]) - 2U_2 \sin \theta \bar{\omega}_\theta] \\ &\quad \left. \left. + 2U_4 h \sin \theta [\bar{\omega} (2f_x - q_x) - 2\bar{\omega}_x] \right\} \right\}, \end{aligned} \quad (\text{A12})$$

$$\begin{aligned} \bar{T}_x^x \equiv \frac{4\pi G}{m_s^2} T_x^x &= \frac{1}{2h^2} e^{-b-f/2-2q} \left\{ e^{5f/2} \csc^2 \theta (\bar{\sigma}_\theta^2 - h\bar{\sigma}_x^2) + e^{f/2+q} h \left[-\bar{\phi}_\theta^2 + \bar{\omega}^2 (-\bar{\sigma}_\theta^2 + h\bar{\sigma}_x^2) + h\bar{\phi}_x^2 \right. \right. \\ &\quad \left. \left. + \bar{\omega} (-2\bar{\sigma}_\theta \bar{\phi}_\theta + 2h\bar{\sigma}_x \bar{\phi}_x) \right] + e^{b/2+3q/2} h^2 \left[2e^f (\bar{X}\bar{V}_x - \bar{Y}\bar{W}_x - \bar{V}\bar{X}_x + \bar{W}\bar{Y}_x) - e^{q/2} \sqrt{h} \sin \theta U_4 \bar{\omega}_x \right] \right\}, \end{aligned} \quad (\text{A13})$$

$$\begin{aligned} \bar{T}_\theta^\theta \equiv \frac{4\pi G}{m_s^2} T_\theta^\theta &= \frac{1}{4h^2} e^{-b-f/2-2q} \left\{ -4e^{b/2+f+3q/2} h^{3/2} (\bar{W}\bar{V}_\theta - \bar{V}\bar{W}_\theta + \bar{Y}\bar{X}_\theta - \bar{X}\bar{Y}_\theta) - 2e^{5f/2} \csc^2 \theta \bar{\sigma}_\theta^2 \right. \\ &\quad \left. + 2e^{f/2} h \left[e^q (\bar{\omega}\bar{\sigma}_\theta + \bar{\phi}_\theta)^2 + e^{2f} \csc^2 \theta \bar{\sigma}_x^2 \right] - e^q h^2 \left[e^{b/2+q} \sin \theta U_2 \bar{\omega}_\theta + 2e^{f/2} (\bar{\omega}\bar{\sigma}_x + \bar{\phi}_x)^2 \right] \right\}, \end{aligned} \quad (\text{A14})$$

$$\begin{aligned} \bar{T}_\varphi^\varphi \equiv \frac{4\pi G}{m_s^2} T_\varphi^\varphi &= \frac{1}{8h^2} e^{-b-3f/2-2q} \left\{ 8e^{b+2f+3q/2} \csc \theta h^{3/2} U_3 (1 + 2\bar{e}\bar{\sigma}) - 4e^{b+5q/2} h^{5/2} \sin \theta U_3 \bar{\omega} [-2\bar{\Omega} + \bar{\omega} + 2\bar{e} (\bar{\phi} + \bar{\sigma}\bar{\omega})] \right. \\ &\quad - 4e^{7f/2} \csc^2 \theta (\bar{\sigma}_\theta^2 + h\bar{\sigma}_x^2) + 4e^{3f/2+q} h [-\bar{\phi}_\theta^2 + \bar{\omega}^2 (\bar{\sigma}_\theta^2 + h\bar{\sigma}_x^2) - h\bar{\phi}_x^2] \\ &\quad \left. + e^{b/2+f+2q} h^{3/2} \left\{ 2 \sin \theta U_4 [2x\bar{\omega} - h(\bar{\omega}[2f_x - q_x] - 2\bar{\omega}_x)] \right. \right. \\ &\quad \left. \left. + \sqrt{h} \left[-2e^{b/2} U_1 (1 + 2\bar{e}\bar{\sigma}) \bar{\omega} + U_2 (\bar{\omega} [2 \cos \theta + \sin \theta (-2f_\theta + q_\theta)] + 2 \sin \theta \bar{\omega}_\theta) \right] \right\} \right\}, \end{aligned} \quad (\text{A15})$$

$$\begin{aligned} \bar{T}_\varphi^t \equiv \frac{4\pi G}{m_s} T_\varphi^t &= \frac{1}{8h} \left\{ 4e^{-3f/2+q/2} h^{3/2} \sin \theta U_3 [2\bar{\Omega} - 2\bar{e}\bar{\phi} - (1 + 2\bar{e}\bar{\sigma}) \bar{\omega}] \right. \\ &\quad \left. + e^{-b/2-f/2} \sqrt{h} \left\{ 2 \sin \theta U_4 [2x - h(2f_x - q_x)] + \sqrt{h} \left[-2e^{b/2} U_1 (1 + 2\bar{e}\bar{\sigma}) + U_2 (2 \cos \theta + \sin \theta [-2f_\theta + q_\theta]) \right] \right\} \right. \\ &\quad \left. + 8e^{-b-q} [\bar{\sigma}_\theta \bar{\phi}_\theta + \bar{\omega} (\bar{\sigma}_\theta^2 + h\bar{\sigma}_x^2) + h\bar{\sigma}_x \bar{\phi}_x] \right\}, \end{aligned} \quad (\text{A16})$$

where

$$U_1 = \bar{X}^2 + \bar{Y}^2 + \bar{V}^2 + \bar{W}^2, \quad U_2 = \bar{X}^2 - \bar{Y}^2 + \bar{V}^2 - \bar{W}^2, \quad U_3 = \bar{X}\bar{Y} + \bar{V}\bar{W}, \quad U_4 = \bar{X}\bar{W} - \bar{Y}\bar{V}.$$

-
- [1] M. Visser, *Lorentzian Wormholes: From Einstein to Hawking* (Woodbury, New York, 1996).
[2] M. Alcubierre and F. S. N. Lobo, *Wormholes, Warp Drives and Energy Conditions*, Fundamental Theories of Physics 189 (Springer, New York, 2017).
[3] K. A. Bronnikov, *Acta Phys. Polon.* **B4**, 251 (1973).
[4] H. G. Ellis, *J. Math. Phys. (N.Y.)* **14**, 104 (1973).
[5] T. Kodama, *Phys. Rev. D* **18**, 3529 (1978).
[6] T. Kodama, L. C. S. de Oliveira, and F. C. Santos, *Phys. Rev. D* **19**, 3576 (1979).
[7] M. S. Morris and K. S. Thorne, *Am. J. Phys.* **56**, 395 (1988).
[8] D. Hochberg and M. Visser, *Phys. Rev. D* **56**, 4745 (1997).
[9] P. E. Kashargin and S. V. Sushkov, *Grav. Cosmol.* **14**, 80 (2008).
[10] P. E. Kashargin and S. V. Sushkov, *Phys. Rev. D* **78**, 064071 (2008).
[11] B. Kleihaus and J. Kunz, *Phys. Rev. D* **90**, 121503 (2014).
[12] X. Y. Chew, B. Kleihaus, and J. Kunz, *Phys. Rev. D* **94**, 104031 (2016).
[13] B. Kleihaus and J. Kunz, *Fundam. Theor. Phys.* **189**, 35 (2017).
[14] X. Y. Chew, V. Dzhunushaliev, V. Folomeev, B. Kleihaus, and J. Kunz, *Phys. Rev. D* **100**, 044019 (2019).
[15] V. Dzhunushaliev, V. Folomeev, B. Kleihaus, and J. Kunz, *Phys. Rev. D* **107**, 044060 (2023).
[16] D. Hochberg, *Phys. Lett. B* **251**, 349 (1990).
[17] N. Furey and A. DeBenedictis, *Class. Quant. Grav.* **22**, 313 (2005).
[18] H. Maeda and M. Nozawa, *Phys. Rev. D* **78**, 024005 (2008).
[19] K. A. Bronnikov, M. V. Skvortsova, and A. A. Starobinsky, *Grav. Cosmol.* **16**, 216 (2010).

- [20] K. A. Bronnikov and J. P. S. Lemos, Phys. Rev. D **79**, 104019 (2009).
- [21] K. A. Bronnikov, V. G. Krechet, and J. P. S. Lemos, Phys. Rev. D **87**, 084060 (2013).
- [22] K. A. Bronnikov and V. G. Krechet, Phys. Rev. D **99**, 084051 (2019).
- [23] K. A. Bronnikov, V. G. Krechet, and V. B. Oshurko, Symmetry **12**, 1306 (2020).
- [24] D. M. Zipoy, J. Math. Phys. **7**, 1137 (1966).
- [25] J. L. Blázquez-Salcedo, C. Knoll, and E. Radu, Phys. Rev. Lett. **126**, 101102 (2021).
- [26] S. Bolokhov, K. Bronnikov, S. Krasnikov, and M. Skvortsova, Grav. Cosmol. **27**, 401 (2021).
- [27] D. L. Danielson, G. Satishchandran, R. M. Wald, and R. J. Weinbaum, Phys. Rev. D **104**, 124055 (2021).
- [28] R. A. Konoplya and A. Zhidenko, Phys. Rev. Lett. **128**, 091104 (2022).
- [29] V. Dzhunushaliev, V. Folomeev, N. Beissen, and A. Nurmukhamedov, Eur. Phys. J. C **86**, 240 (2026).
- [30] C. Herdeiro, I. Perapechka, E. Radu, and Y. Shnir, Phys. Lett. B **797**, 134845 (2019).
- [31] C. Herdeiro, I. Perapechka, E. Radu, and Y. Shnir, Phys. Lett. B **824**, 136811 (2022).
- [32] F. Finster, J. Smoller, and S. T. Yau, Phys. Rev. D **59**, 104020 (1999).
- [33] V. Dzhunushaliev and V. Folomeev, Phys. Rev. D **99**, 084030 (2019).
- [34] V. Dzhunushaliev and V. Folomeev, Phys. Rev. D **99**, 104066 (2019).
- [35] J. L. Blázquez-Salcedo and C. Knoll, Eur. Phys. J. C **80**, 174 (2020).
- [36] C. Armendariz-Picon and P. B. Greene, Gen. Rel. Grav. **35**, 1637 (2003).
- [37] I. Lawrie, *A Unified Grand Tour of Theoretical Physics* (Institute of Physics Publishing, Bristol, 2002).
- [38] V. Dzhunushaliev and V. Folomeev, Eur. Phys. J. C **84**, 129 (2024).
- [39] N.I.M. Gould, J.A. Scott, Y. Hu, ACM Trans. Math. Softw. **33**, 10 (2007);
O. Schenk, K. Gartner, Future Gener. Comput. Syst. **20**, 475 (2004).
- [40] V. Dzhunushaliev and V. Folomeev, Eur. Phys. J. C **86**, 382 (2026).
- [41] J. L. Friedman, L. Parker, and J. R. Ipser, Astrophys. J. **304**, 115 (1986).
- [42] C. A. R. Herdeiro, A. M. Pombo, and E. Radu, Phys. Lett. B **773**, 654 (2017).
- [43] J. Wheeler, *Geometrodynamics* (New York: Academic Press, 1963).
- [44] A. Y. Burinskii, Phys. Usp. **67**, 1034 (2024).